

On-target Inhibition of Tumor Fermentative Glycolysis as Visualized by Hyperpolarized Pyruvate¹

Pankaj Seth², Aaron Grant², Jian Tang, Elena Vinogradov, Xiaoen Wang, Robert Lenkinski and Vikas P. Sukhatme

Department of Medicine, Divisions of Interdisciplinary Medicine and Biotechnology, Renal and Hematology–Oncology, and Department of Radiology, Beth Israel Deaconess Medical Center, Harvard Medical School, Boston, MA, USA

Abstract

Many cancer cells display the Warburg effect, that is, enhanced glycolysis followed by fermentation (conversion of pyruvate to lactate). Recently, the molecular basis for these effects has started to be elucidated, and the up-regulation of the lactate dehydrogenase A (LDH-A) isoform of lactate dehydrogenase is felt to be a major molecular mediator of this phenomenon. Moreover, LDH-A expression in tumor tissue and LDH-A levels in blood portend a bad prognosis, and LDH-A blockade can lead to tumor growth inhibition in tumor transplant models. We have extended existing data (some of which were published during the time when we were carrying out our studies) in two important ways: 1) inhibition of LDH-A in a glycolytic lung cancer cell line results in reactive oxygen species-mediated apoptosis and increased sensitivity to the chemotherapeutic drug paclitaxel and 2) inhibition of fermentative glycolysis can also be accomplished by activation of the pyruvate dehydrogenase complex by the drug dichloroacetate, now undergoing clinical trials, and that this phenomenon can be monitored *in vivo* in a noninvasive real-time manner through magnetic resonance spectroscopy using hyperpolarized pyruvate. Collectively, these data suggest that *in vivo* effects of drugs that redirect the fate of pyruvate, and hence are aimed at reversing the Warburg effect, could be monitored through the use of hyperpolarized magnetic resonance spectroscopy, a method that is scalable to human use.

Neoplasia (2011) 13, 60–71

Introduction

Many cancer cells display enhanced glycolysis followed by fermentation (conversion of pyruvate to lactate), known as the Warburg effect [1]. Recently, the molecular basis for these effects has started to be elucidated: part of it relates to the induction of the so-called hypoxia-inducible factor 1 alpha (HIF-1 α), which occurs as a consequence of hypoxia and alterations in certain oncogenes or tumor suppressor genes. For example, activation of the *myc* and *ras* oncogenes or loss of tumor suppressor genes such as *VHL* (von Hippel Lindau) and *FH* (fumarate hydratase) elevates HIF-1 α levels. Increased HIF expression results in the increased transcription of genes involved in glucose transport, glucose metabolism, lactate formation (through activation of lactate dehydrogenase-A [LDH-A]—see below) [2,3] and lactate export from cells [4]. HIF is also thought to block the entry of pyruvate into the Krebs cycle by inhibiting the pyruvate dehydrogenase (PDH) complex [5]. In addition, recent discoveries on the p53 tumor suppressor also

suggest that this protein can regulate glucose metabolism. p53 mutations result in diminished oxidative phosphorylation [6]. Collectively, these studies provide an explanation for the Warburg effect.

Abbreviations: LDH-A, lactate dehydrogenase A; HIF, hypoxia-inducible factor; DCA, dichloroacetate; MR, magnetic resonance; PDK, pyruvate dehydrogenase kinase; PDH, pyruvate dehydrogenase; MCT, monocarboxylate transporter; NMR, nuclear magnetic resonance; ROS, reactive oxygen species; NAC, *N*-acetyl cysteine

Address all correspondence to: Vikas P. Sukhatme, MD, PhD, Division of Interdisciplinary Medicine and Biotechnology, GZ602, Beth Israel Deaconess Medical Center, 330 Brookline Ave, Boston, MA 02215. E-mail: vsukhatm@bidmc.harvard.edu

¹This work was partly supported by seeds funds to V.P.S. and P.S. P.S. is supported by the National Institutes of Health grant K01CA104700. Part of this work was also supported by a Harvard Clinical and Translational Science Award collaborative pilot research project to A.G., P.S., R.L., and V.P.S.

²These authors have contributed equally.

Received 19 July 2010; Revised 25 September 2010; Accepted 28 September 2010

Copyright © 2011 Neoplasia Press, Inc. All rights reserved 1522-8002/11/\$25.00
DOI 10.1593/neo.101020

The lactate dehydrogenases are involved in the interconversion of pyruvate and lactate. There are two LDH subunits encoded by two separate genes, *LDH-A* and *LDH-B*. These two subunits associate to form five different isoforms of tetrameric LDH: LDH1 (LDH-B4), LDH2 (LDH-B3A1), LDH3 (LDH-B2A2), LDH4 (LDH-B1A3), and LDH5 (LDH-A4). LDH1 is effective in the conversion of lactate into pyruvate, whereas LDH5 is effective in the conversion of pyruvate into lactate. The observation that HIF-1 α increases fermentation is likely mediated by the induction of LDH-A [7–9]. LDH-A is upregulated not only by HIF and c-Myc at a transcriptional level but also by protein kinase A and protein kinase C at the messenger RNA stability level [10,11].

The notion that LDH-A may regulate tumor growth is suggested by studies that LDH-A overexpression in non-small cell lung cancer (NSCLC) is linked to tumor hypoxia, angiogenic factor production, and poor prognosis [8], and similar data have been shown in colorectal cancer [7]. Increased LDH-A expression also results in increased extracellular acidity because the extrusion of lactate is accompanied by proton transport through one of several monocarboxylate transporters (MCTs) [12,13]. It has now been documented that reduction of fermentative glycolysis through LDH-A blockade results in reduced tumor growth, implicating LDH-A as another viable therapeutic target for tumorigenesis [14,15]. Therefore, we asked whether inhibition of LDH-A in the highly glycolytic NSCLC cell line A549 results in reduced tumor growth. Moreover, we asked whether we could visualize the decrease in pyruvate to lactate flux in a noninvasive real-time manner. Because we did not have access to LDH-A inhibitors, we asked whether the inhibition of fermentative glycolysis as measured by decreased pyruvate to lactate flux can be achieved by activation of PDH by dichloroacetate (DCA) that will shuttle pyruvate toward tricarboxylic acid cycle (TCA) and away from LDH-A catalyzed reaction.

DCA is a small molecule of 150 Da. *In vitro*, DCA activates PDH by inhibiting PDH kinase (PDK) at concentrations of 10 to 250 μ M depending on the isoform [16]. The isozyme PDKII is expressed constitutively in most tissues and is the most sensitive to DCA [17]. The enhanced PDH activity diverts metabolism from fermentative glycolysis to glucose oxidation and decreases mitochondrial membrane potential polarization, resulting in the opening of mitochondrial transition pores. This allows for the translocation of reactive oxygen species and cytochrome *c* from the mitochondria to the cytoplasm, inducing apoptosis through the activation of caspases. DCA has undergone extensive clinical trials for lactic acidosis, sepsis, burns, and cirrhosis with doses ranging from 25 to 100 mg/kg per day orally or intravenously [18,19]. So far, no major adverse effects of DCA treatment at these doses have been reported, except peripheral neuropathy, which was reversible on drug discontinuation (reviewed in Root et al. [35]). Recent work also shows that facilitation of pyruvate oxidation by DCA treatment leads to tumor growth reduction in many solid tumors *in vitro* and *in vivo*, including NSCLC, glioblastoma, and prostate cancer [20,21]. DCA is in clinical trials for glioblastoma, NSCLC, and breast cancer (clinicaltrials.gov).

To assess the response of tumors to administration of DCA, we made use of hyperpolarized nuclear magnetic resonance (NMR) spectroscopy to noninvasively monitor the conversion of pyruvate into lactate. Until recently, studies of *in vivo* metabolism using NMR have been hampered by the low intrinsic sensitivity of the method. The advent of practical techniques for preparing liquid solutions of hyperpolarized 13 C-labeled metabolites [22,23] has yielded dramatic increases in sensitivity, making it possible to perform real-time imaging and spectroscopy of metabolism. [$1-^{13}$ C]pyruvate is readily hyperpolarized using dynamic nuclear

polarization, and rapid conversion of pyruvate into lactate is observed *in vivo* [24]. Although it has been argued that the lactate signal is at least partially due to exchange of the 13 C label between hyperpolarized pyruvate and the endogenous lactate pool, rather than net synthesis of lactate [25,26], this method provides a measure of both the size of the endogenous lactate pool and the activity of LDH. In addition, transport of pyruvate by MCT1 has been shown to play an important role in lactate formation in cell culture [27]. Studies making use of hyperpolarized pyruvate in TRAMP mice (a murine model of prostate cancer) have shown that lactate signal increases with cancer progression and correlates with tumor histologic grade [28]. Moreover, data from a murine EL-4 lymphoma model show that the lactate signal is reduced after chemotherapeutic intervention [25]. Other recent studies have shown that inhibition of phosphatidylinositol 3-kinase also leads to reduced lactate signal [29]. Pyruvate is only one of several substrates that can be studied using these techniques; other metabolites including fumarate [30], acetate [31], succinate [32] choline [33], and fructose [34] have also been described.

As emphasized above, the lactate signal obtained after administration of hyperpolarized pyruvate is determined by several factors. Chief among these is the so-called “exchange” signal, which results from exchange of the 13 C label between the injected pyruvate and the endogenous lactate pool. This signal can be sizeable even when there is little or no net conversion of pyruvate into lactate and depends on both the activity of LDH and the size of the endogenous lactate pool. Indeed, previous studies in cell culture have shown that addition of exogenous, unlabeled lactate results in an increase in lactate signal after administration of hyperpolarized pyruvate [25]. Consequently, interventions that reduce levels of endogenous lactate will result in reduced lactate signal even if the activity of LDH is unchanged. By contrast, the flux of pyruvate through PDH, which produces acetyl-CoA and labeled bicarbonate, does not possess a similar exchange component. The bicarbonate signal is a direct measure of net flux through PDH, which is typically much smaller than the exchange process that accounts for much of the lactate signal. Indeed, it was not until the work of Kohler et al. [24] that bicarbonate was routinely detected with spectroscopic imaging, and even then the signal was quite small in comparison to the lactate signal. These observations have special relevance to studies of metabolism in the Warburg effect, where interventions that shift pyruvate metabolism away from lactate and toward acetyl-CoA are sought. In particular, when such interventions reduce the size of the endogenous lactate pool, they will result in reduced lactate exchange signal. However, this reduction in lactate signal need not be accompanied by a proportionate increase in bicarbonate signal; indeed, there is no reason to expect lactate exchange rates to be directly correlated with total PDH flux.

Materials and Methods

Chemicals and Reagents

Cell culture medium was purchased from American Type Culture Collection (ATCC, Manassas, VA). 2-Deoxy-D-glucose and lentiviral constructs were purchased from Sigma Aldrich (St Louis, MO), and viral power kit and packaging cell line 293FT were purchased from Invitrogen (Carlsbad, CA). Sheep polyclonal LDH-A antibodies were purchased from Abcam (Cambridge, MA). Rabbit polyclonals for activated caspase-3 and activated poly (ADP-ribose) polymerase (PARP) were purchased from Cell Signaling (Cambridge, MA). The assay kit for measuring ATP was purchased from Roche (Indianapolis, IN). The

lactate measurement kit was purchased from CMA microdialysis (N. Chelmsford, MA). Cell cycle reagents and annexin V assay kits were purchased from Guava Technologies (Hayward, CA). Athymic mice for tumor implantation were purchased from Charles River Laboratories (Wilmington, MA). A549 cells were maintained in Ham's F12 medium with glutamine and sodium pyruvate with 10% fetal calf serum (Sigma-Aldrich). The hypoxic conditions (0.1%-0.5% O₂) were maintained in a controlled atmosphere chamber (Billups-Rothenberg, Del Mar, CA) at 37°C in certified 5% CO₂/94.5% nitrogen.

Generation of LDH-A-Deficient Cell Lines

A549 cells were infected with empty small hairpin RNA (shRNA) vector control and three different LDH-A shRNA lentiviruses as described [35]. Briefly, recombinant lentivirus particles were produced by transient transfection of 293T cells. Subconfluent 293FT cells were cotransfected with 3 µg of an shRNA plasmid, and 9 µg of viral power packaging mix (an optimized proprietary mix of three plasmids, pLP1, pLP2, and pLP/VSVG from Invitrogen) using Lipofectamine 2000 (Invitrogen). After 16 hours, the culture medium was switched to a regular growth medium, and cells were allowed to incubate for an additional 48 hours. Conditioned cell culture medium containing recombinant lentiviral particles was harvested and frozen. A549 cells were treated with the above cell culture supernatant containing lentiviral particles for 24 hours. These cells were then selected in puromycin (Sigma-Aldrich) to generate stable cell lines encoding empty vector shRNA and LDH-A shRNA. The selected cell lines were validated for diminished LDH-A expression by Western blot analysis. Briefly, total cellular proteins were separated by SDS-PAGE and electrotransferred to polyvinylidene fluoride membranes and immunoblotted with anti-LDH antibody overnight at 4°C. After washing with TBS-T, the membrane was incubated with secondary antibody for 30 minutes. Protein bands were detected using SuperSignal West Pico Chemiluminescent substrate from Pierce (Rockford, IL). To demonstrate that shRNA is specific for LDH-A *versus* B isoform, we obtained HCCT 116 cells that are deficient in methyltransferases and express LDH-B [36,37] (LDH-B is hypermethylated and hence not expressed in most cancer cells [38]). These HCCT 116 cells deficient in methyltransferases, known as DKO cells [36], were used for shRNA-mediated LDH-A knockdown as described above.

Proliferation Assay

Control and LDH-A-deficient cell lines were plated in 60-mm dish at a density of 1×10^5 cells/dish in HAM's F12 medium supplemented with 10% FBS for 24 hours at 37°C in a 5% CO₂ incubator. After 24, 48, 72, 96, and 120 hours of initial plating, cells were scraped, washed with PBS and resuspended in 1 ml of Hanks' buffer, and counted. All samples were assayed in duplicate to generate proliferation curves as described [5]. For proliferation assays done in hypoxia, the hypoxic conditions (0.1%-0.5% O₂) were maintained in a controlled atmosphere chamber (Billups-Rothenberg) at 37°C in certified 5% CO₂/94.5% nitrogen.

Lactate Accumulation

To assess whether LDH-A-deficient cell lines have a diminished accumulation of lactate, we measured lactate accumulation in control and LDH-A-deficient cell lines as described [39]. Briefly, the cell culture-conditioned supernatant was used to measure lactate levels by a simple calorimetric analysis based on the reduction of the tetrazolium salt INT in a nicotinamide adenine dinucleotide (NADH)-coupled enzymatic

reaction to formazan, which is water-soluble and exhibits an absorption maximum at 492 nm. The intensity of the red color formed is proportional to the lactate concentration in the conditioned medium.

Cell Cycle Analysis

Cells were fixed in 70% ethanol, stained with cell cycle reagent (Guava Technologies, Hayward, CA), and subjected to fluorescence-activated cell sorting on an EasyCite Plus flowcytometer (Guava Technologies).

Intracellular ATP

Intracellular ATP levels in control and LDH-A-deficient cells were measured according to the manufacturer's instructions. In brief, cell lysates were collected, and luminescence was measured using a luminescence reader (Molecular Devices, Sunnyvale, CA) and normalized to protein concentration.

Annexin V Assay

Apoptosis was measured by Guava PCA-96 Nexin (Guava Technologies) as per the manufacturer's protocol. Briefly, cells were harvested and resuspended in $1 \times$ Nexin buffer with annexin V-PE, and Nexin 7-AAD. The cells were allowed to incubate for 15 minutes and analyzed in the Guava flow cytometer.

LDH Enzyme Activity

LDH-A activity was measured in the direction of reduction of pyruvate to lactate by monitoring the changes in the absorbance of NADH at 340 nm, 25°C in potassium phosphate buffer, pH 7.4. Briefly, the reaction mixture contained 50 mM potassium phosphate buffer (pH 7.4) and pyruvate (200 µM). The reaction was initiated by the addition of cell extract prepared in potassium phosphate buffer and NADH (250 µM), and decrease in absorbance at 340 nm was monitored every 4 minutes.

Oxygen Consumption and Proton Production Rate Analysis

The XF24 Extracellular Flux analyzer (Seahorse Biosciences, Billerica, MA) is a fully integrated 24-well instrument that measures in real-time the uptake and release of metabolic end products. Each XF24 assay well contains a disposable sensor cartridge, embedded with 24 pairs of fluorescent biosensors (oxygen and pH), coupled to fiber-optic waveguides. The waveguides deliver light rays at various excitation wavelengths (oxygen = 532 nm, pH = 470 nm) and transmit a fluorescent signal (oxygen = 650 nm, pH = 530 nm) to a set of highly sensitive photodetectors. This technology was used to measure oxygen consumption (OCR) and proton production rate (PPR), both expressed in picomoles per minute in control and LDH-A-deficient cell lines as described [40].

Soft Agar Growth Assay

Sixty-millimeter plates were layered with 1.4% agarose in phenol red-free 2× DMEM and allowed to solidify. A549 cells expressing control shRNA and LDH-A shRNA were mixed in 0.8% agarose in 2× DMEM and seeded onto these 1.4% agarose layers (30,000 cells per plate). These plates were allowed to solidify for 15 minutes and were covered with growth medium. The growth medium was changed every 3 days for 4 weeks. Cells were washed with PBS and fixed in 100% methanol for 30 minutes followed by staining with 0.5% crystal violet for 1 hour. The plates were washed with PBS, and colonies with size greater than 0.5 mm were counted under the microscope. The experiment was performed in triplicates, and four random fields per dish were counted. Results represent two independent experiments.

Reactive Oxygen Species Measurements

Intracellular reactive oxygen species (ROS) production was measured by staining with dichlorodihydrofluorescein diacetate (CM-H₂DCFDA; Invitrogen). CM-H₂DCFDA is a cell-permeant indicator for reactive oxygen species that is nonfluorescent until removal of the acetate groups by intracellular esterases and oxidation occurs within the cell. The procedure for measuring ROS was carried out as described earlier [5], with minor modification. Briefly, cells were loaded with 5 μ M H₂DCFDA for 1 hour, washed in PBS, and incubated in fresh medium for 30 minutes. The cells were then subjected to FACS analysis.

Tumor Implantation

A total of 5×10^6 control and LDH-A-deficient cells (LDH-A shRNA no. 1) were subcutaneously implanted in eight athymic mice. The implantation was done such that each mouse had control cells on the right flank and LDH-A-deficient cells on the left flank. Similarly, 5×10^6 control and LDH-A-deficient cells (LDH-A shRNA no. 2) were subcutaneously implanted in the flanks of eight athymic mice. Tumors were measured every 7 days, and tumor volume was calculated as described before [41]. Tumor lysates were prepared by homogenization of tumor tissues in lysis buffer and were separated by SDS-PAGE and electrotransferred to PDVF membranes and immune blotted with anti-LDH antibody as described above. For DCA administration experiments, 5×10^6 A549 wild type cells were implanted in athymic mice that were then administered DCA as described below.

TUNEL Assay

Tumor tissue from control and LDH-A-deficient tumors were embedded in paraffin and assayed for apoptosis through terminal deoxynucleotidyl transferase dUTP nick end labelling (TUNEL) staining as described earlier [42].

Administration of DCA

The amount of 25 mg/kg DCA was administered 24 hours before the pyruvate imaging through interperitoneal injection. Another dose of 25 mg/kg was given just before imaging intravenously by tail vein injection.

Magnetic Resonance Imaging and Spectroscopy

Modifications of tumor metabolism in A549 xenograft tumors resulting from administration of DCA were assessed using ¹³C NMR spectroscopy after administration of hyperpolarized ¹³C₁-pyruvate.

Preparation of Hyperpolarized Pyruvate

Hyperpolarized pyruvate was prepared as described previously [24]. Pyruvic acid was combined with 15 mM trityl radical (OX063; GE Healthcare, London, UK), and 27.7 ± 0.4 mg of this mixture was then placed in an open sample cup. The cup was placed inside a commercial hyperpolarizer (Oxford Hypersense; Oxford Instruments, Oxfordshire, UK) where it was frozen at 1.4 K and subjected to microwave radiation at 50 to 100 mW and a frequency of approximately 94.110 GHz. Solid-state ¹³C NMR was used to monitor the growth of the carbon polarization. The microwave power was set to 100 mW provided that the system could maintain a temperature of 1.4 K at this power level. Otherwise, the power was reduced to 50 mW. If the system was unable to maintain 1.4 K at 50 mW, it was "baked out" to remove impurities from the variable temperature insert and restore its ability to maintain a temperature

of 1.4 K. The choice of microwave power was found to have a negligible impact on the solid-state polarization buildup. All samples were polarized for a minimum of 40 minutes, by which time the solid-state polarization had reached at least 95% of its maximum, saturated value. The pyruvic acid was then thawed and ejected from the system using 4 ml of hot USP saline solution (0.45% NaCl) containing 40 mM Tris and 25 mg/100 ml disodium EDTA. The sample was collected in a glass container and mixed with a sufficient quantity of 1N sodium hydroxide solution to obtain a pH of 7.5 ± 0.5 . The resulting solution contained approximately 78 mM hyperpolarized pyruvate.

Animal Preparation

Each mouse was anesthetized using inhaled isoflurane (2%-3%) in a drop box and then transferred to a work area where anesthesia was maintained by isoflurane delivered through a nose cone. A catheter connected to a narrow extension tube was placed in the tail vein, and a small ¹³C surface coil was placed over the xenograft tumor (see below). The mouse was then placed inside a 4.7-T horizontal bore scanner (Bruker Biospec, Billerica, MA). Proper levels of anesthesia were maintained using respiratory monitoring (small animal monitoring system; SAI, Stony Brook NY) throughout the imaging study.

Magnetic Resonance Imaging and ¹³C Spectroscopy

Conventional proton magnetic resonance imaging (MRI) was used to assess the size and location of the xenograft tumors and to verify the location of the ¹³C surface coil. Axial T₂-weighted images were acquired using a RARE sequence (TR/TE = 1000/23 milliseconds) with echo train length 4, 128 \times 128 matrix, 4 \times 4 cm² field of view, and 1-mm slice thickness.

¹³C spectroscopic measurements of pyruvate metabolism in the xenograft tumors were performed using surface coil localized spectroscopy. Depending on the size of the tumor, one of two circular surface coils was used: a 10-mm-diameter coil was used for larger tumors, and a 6-mm-diameter coil was used for smaller tumors. Signals acquired from the surface coils were dominated by metabolites within the tumor owing to the placement of the coils and their small diameters. The coils were operated in a transmit/receive mode. A crude estimate based on a Biot-Savart calculation shows that in this configuration, on the axis of the coil, just more than 90% of the NMR signal is derived from the tissue within a depth of one coil radius from the surface of the body, corresponding to 3 to 5 mm for the 6- and 10-mm-diameter coils, respectively. Although imperfect coil placement may result in stray signals from tissue in the vicinity of the tumor, this technique is expected to yield signals that are dominated by tissue within the tumor. The location of the coil with respect to the tumor was validated by means of an MRI-visible marker consisting of roughly 1 cm of rubber tubing, 1/8 in. outside diameter, which was filled with water, sealed, and affixed to the coil along its center axis. This tubing was readily visible in the axial T₂-weighted proton images described above, which were used to verify that the coil was centered within 1 to 2 mm of the center of the tumor.

Before the imaging studies, the ¹³C radiofrequency transmit power was adjusted by placing the surface coil on a phantom containing 3 M ¹³C-labeled sodium acetate in water. ¹³C spectra were acquired from the phantom at a range of transmit power values, and the relative signal strength for each value was measured. For *in vivo* studies, the transmit power was set to a relatively low value that yielded approximately 1/10th to 1/20th of the peak signal. This low transmit power corresponds to a low average flip angle over the sensitivity region of the coil. With these settings, the hyperpolarized magnetization was minimally disturbed

by the application of radiofrequency pulses, and it was possible to acquire dozens of spectra during a period of minutes after administration of hyperpolarized pyruvate.

After imaging the tumor and verifying the placement of the ^{13}C surface coil, 300 μl of hyperpolarized pyruvate solution, described above, was administered through the tail vein catheter. Just before the injection, an automated script was initiated on the MRI scanner that acquired a ^{13}C spectrum from the surface coil every 5 seconds with spectral width 200.11 ppm, 8192 points, and total acquisition time of 812.65 milliseconds.

Data Analysis

The ^{13}C spectra were apodized with a 15-Hz line-broadening filter, phased, and baseline-corrected using software provided with the MRI scanner (Bruker TopSpin). The spectral lines corresponding to pyruvate, lactate, and alanine were then integrated and plotted as a function of time. All of the signals were scaled by a common factor to obtain a peak pyruvate signal equal to 1. The maximum lactate signal (after scaling) was used as a measure of the relative lactate formation in each tumor. (Owing to the scaling procedure, the lactate signal can also be thought of as the maximum lactate signal divided by the maximum pyruvate signal.) The lactate signals for untreated tumors and DCA-treated tumors were then compared using a two-tailed *t* test.

Results

Generation and Validation of LDH-A-Deficient Cell Lines

To investigate the effects of diminished LDH-A expression, we chose to work with A549 cells, a highly glycolytic NSCLC cell line. A549 cells are highly glycolytic as shown by their susceptibility to 2-deoxy-D-glucose, a well-characterized glucose analogue, which can be phosphorylated in the first step of glycolysis but cannot undergo additional glycolytic reactions. We saw a concentration-dependent fall in cellular ATP levels with addition of increasing amounts of 2-deoxy-D-glucose to the culture medium (Figure 1A). We generated LDH-A-deficient A549 stable cells using RNA interference technology. Western blot analysis with anti-LDH-A antibody (Figure 1B) demonstrated that cell line nos. 1 and 2, representing shRNAs targeting two different regions within the LDH-A messenger RNA, have diminished LDH-A protein expression compared with the cell line expressing control shRNA. We chose to pursue further analysis with shRNA no. 1 and shRNA no. 2. ShRNA-mediated knockdown of LDH-A in DKO cells does not affect LDH-B expression and confirmed specificity of LDH-A versus LDH-B inhibition (Figure 1C). The LDH-A-deficient cells compared with control cells had low enzyme activity (Figure 1D), resulting in low lactate levels (Figure 1E). Oxamate, a nonspecific LDH inhibitor, served as a positive control in these experiments. PPR analysis

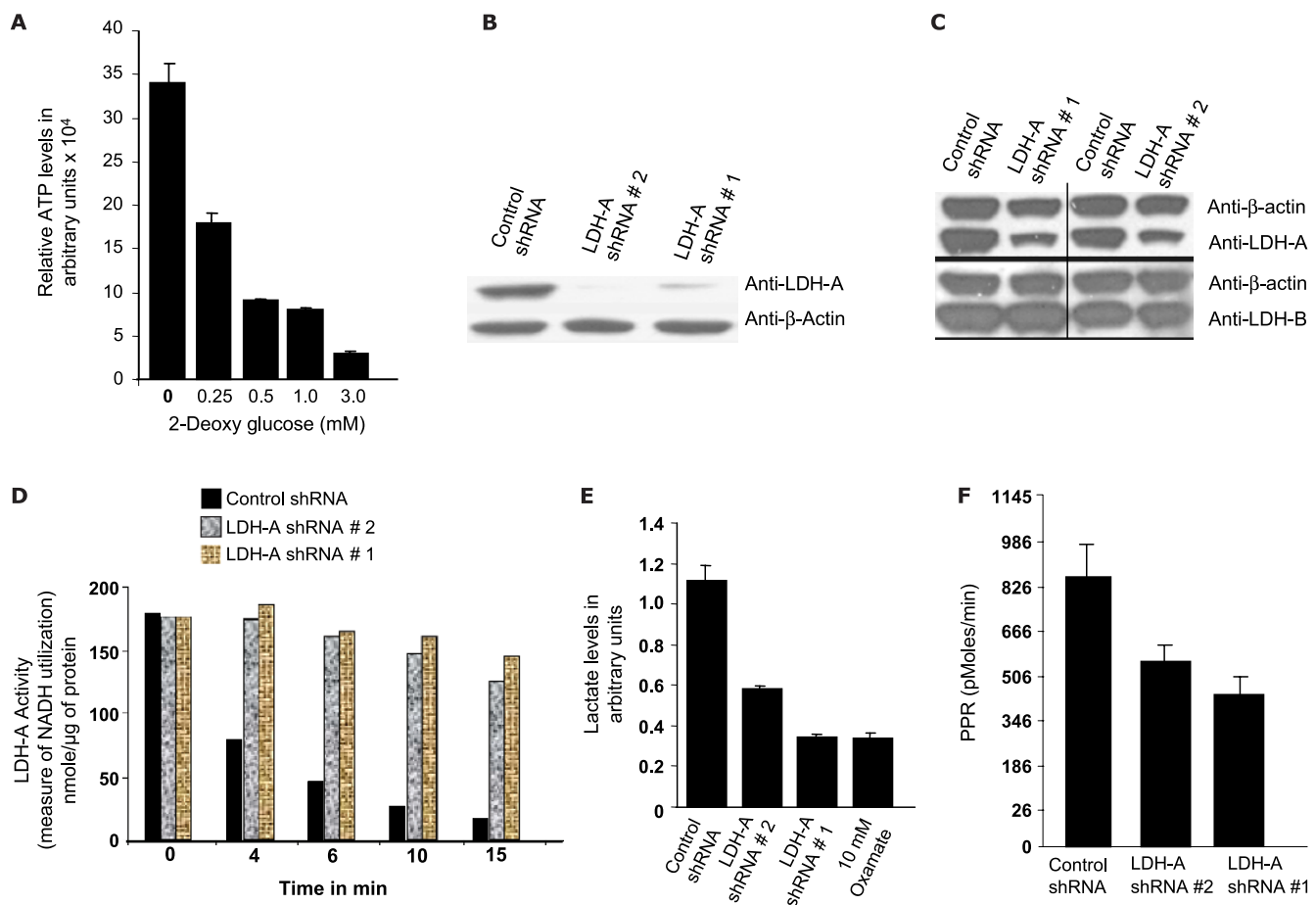


Figure 1. (A) Relative ATP levels in A549 cells in the presence of increasing concentrations of 2-deoxy-D-glucose. (B) Western blot analysis of A549 LDH-A-deficient cell lines using LDH-A antibody. (C) Western blot analysis with LDH-A and LDH-B specific antibody on control versus LDH-A-deficient DKO cells. (D) LDH activity measurements in control and A549 LDH-A-deficient cell lines. (E) Lactate levels in control and A549 LDH-A-deficient cell lines. (F) PPR in control and A549 LDH-A-deficient cell lines as measured by the XF24 analyzer.

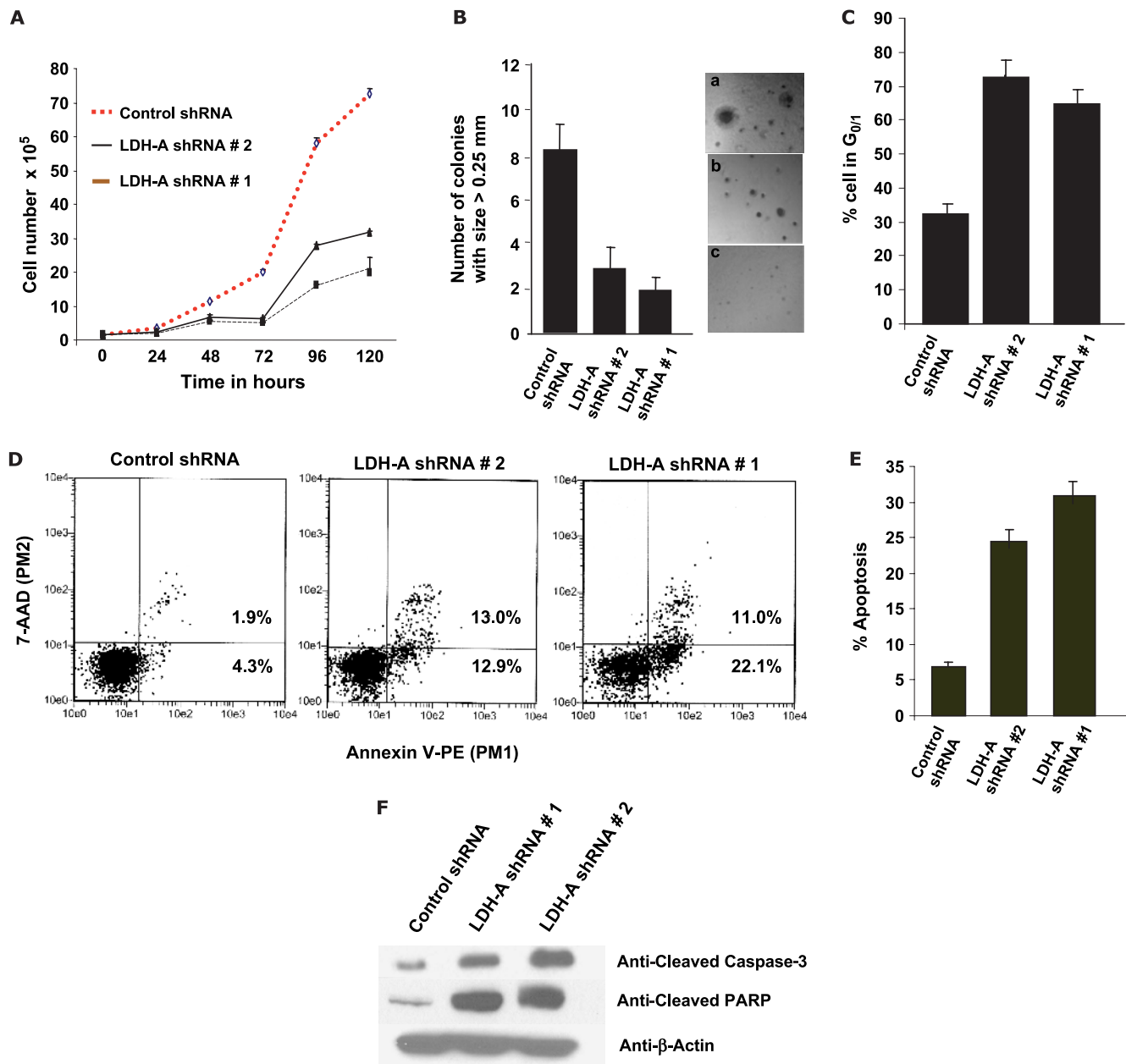


Figure 2. (A) Proliferation assay analysis of A549 LDH-A-deficient cell under normoxia. (B) Soft agar colony assay for A549 LDH-A-deficient cell lines *versus* control cell line. (C) Cell cycle analysis (percent cells in G_{0/1} in control and LDH-A-deficient cell lines. (D and E) Apoptosis as measured by annexin V and its representation in bar format. (F) Western blot analysis in control and A549 LDH-A-deficient cell lines for activated caspase-3 and activated PARP.

of the control cell line and LDH-A-deficient cells with the XF24 analyzer also showed that LDH-A-deficient lines produced less extracellular acidification as measured through lactate accumulation assay (Figure 1F).

In Vitro Characterization of LDH-A-Deficient Cell Lines

To test whether cell lines deficient in LDH-A expression would show altered cell proliferation, we characterized these stable cell lines in various *in vitro* assays. As shown in Figure 2A, the LDH-A-deficient cell lines display a proliferation defect of varying degree. To access the growth potential in three dimensions, we used a soft agar growth assay. LDH-A-deficient cells generated smaller colonies compared with the control shRNA cell line, suggesting a lower tumorigenic potential (Figure 2B).

LDH-A-deficient cells also demonstrated significantly higher percentage of cells in G_{0/1} state (Figure 2C) as well as increased apoptosis compared with the cells infected with control shRNA (Figure 2C). Viable cells do not bind annexin V-PE or 7-aminoactinomycin D (7AAD) as reflected in the lower left-hand quadrant of the dot plot. Apoptotic cells with exposed PS but intact cell membranes bind annexin V-PE but exclude 7AAD. Fluorescence from this population is reported in the lower and upper right-hand quadrant. Induction of apoptosis is also demonstrated by Western analysis of cleaved caspase-3 (Figure 2, D and E) and cleaved PARP in LDH-A-deficient cell lines (Figure 2F).

Because hypoxic regions in tumors must rely on glycolysis, especially fermentative glycolysis regulated by LDH-A, an HIF-1 α target, we asked whether cells with diminished LDH-A expression *versus* control

cells would behave differently in hypoxic conditions. The proliferation rate in a hypoxic environment is significantly slower in control as well as LDH-A-deficient cells, with LDH-A-deficient cells showing comparatively more reduced growth (Figure 3A).

To determine the impact on ATP levels of LDH-A inhibition, ATP levels were measured under normoxic and hypoxic conditions. In comparison to the control cell line, LDH-A-deficient cells do not show significant ATP depletion (~10% reduction) in normoxic condition, suggesting that a functional OXPHOS is able to compensate for decreased fermentative activity. On other hand, in hypoxic conditions, the ATP levels were significantly decreased (~40%) in LDH-A-deficient cells (Figure 3B). This is in agreement with the substantially reduced proliferation rate observed in hypoxic conditions.

We were unable to see a significant increase in NADH/NAD⁺ ratio in our LDH-A-deficient cell lines (data not shown). These results are in line with our observation of an increased rate of oxygen consumption in LDH-A-deficient cells and suggest enhanced activation of OXPHOS as a result of LDH-A knockdown (Figure 3C).

In Vivo Characterization of LDH-A-Deficient Cell Lines

On the basis of our *in vitro* results, we hypothesized that LDH-A-deficient cell lines might have significantly diminished growth *in vivo*. We found that both of our two independent LDH-A knockdown cell lines showed marked growth retardation in nude mice (Figure 4, A and B; each mouse injected with both control shRNA and LDH-A knockdown cells in the flank). Also shown is the Western blot analysis of tumor tissue isolated from these tumors to demonstrate LDH-A knockdown in tumor tissue. As in our *in vitro* data, the tumor tissue arising from LDH-A-deficient cells showed increased apoptosis as measured by TUNEL staining (Figure 4C) and an assessment of the average number of apoptotic cells in four random areas TUNEL staining (Figure 4D).

Increased ROS Generation in LDH-Deficient Cells Mediates Apoptosis

On the basis of the observed increase in oxygen consumption in LDH-A-deficient cells, we asked whether enhanced OXPHOS would lead to increased formation of reactive oxygen species perhaps as a consequence of increased electron flow. We found increased ROS levels in the LDH-A-deficient cells compared with control (Figure 5A). Furthermore, this ROS generation could be blocked by the antioxidant *N*-acetyl cysteine (NAC), and this not only neutralized the ROS generation but also led to significant rescue from apoptosis as measured by cleaved PARP (Figure 5B). These data suggest that increased ROS formation occurs in LDH-A-deficient cells, and this increase is responsible for the observed increase in cell death.

LDH-A Inhibition Sensitizes A549 Cells to Low Dose Paclitaxel

Increased extracellular acidity resulting from increased fermentative glycolysis has been suggested to be responsible for more aggressive metastatic behavior [9,43,44], resistance to immune recognition [45–47], and resistance to chemotherapy [48,49]. In fact, a recent report showed that NSCLC patients with enhanced LDH-A expression were resistant to chemotherapy treatment [8]. Therefore, we also asked whether inhibition of fermentative glycolysis can increase the efficacy of a chemotherapeutic drug such as paclitaxel, a chemotherapeutic drug used in the therapy for NSCLC. Apoptosis even at low paclitaxel concentrations was enhanced (Figure 6A; graphical representation in Figure 6B).

LDH-A Inhibition Is Functionally Similar to PDH Activation

Because PDH is negatively regulated by PDK enzymes (schematic no. 1), we asked whether knockdown of PDK II resulting in PDH activation might give us results similar to those noted with LDH-A inhibition. We found that the level of OCR and ROS was significantly higher in A549 cells with reduced PDK II expression compared with

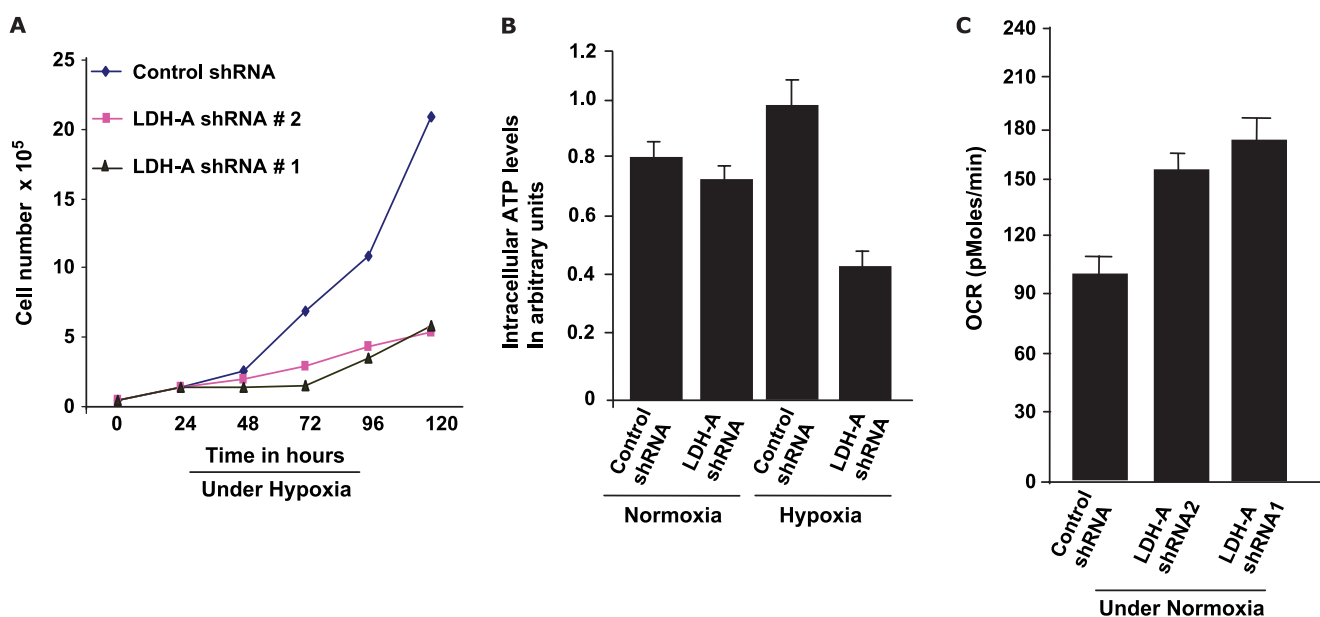


Figure 3. (A) Proliferation assay analysis of A549 LDH-A-deficient cell lines in hypoxic conditions. (B) Intracellular ATP levels under normoxic and hypoxic condition in control and LDH-A-deficient cells. (C) Oxygen consumption rate in control and LDH-A-deficient cell lines as measured by XF24 analyzer under normoxia.

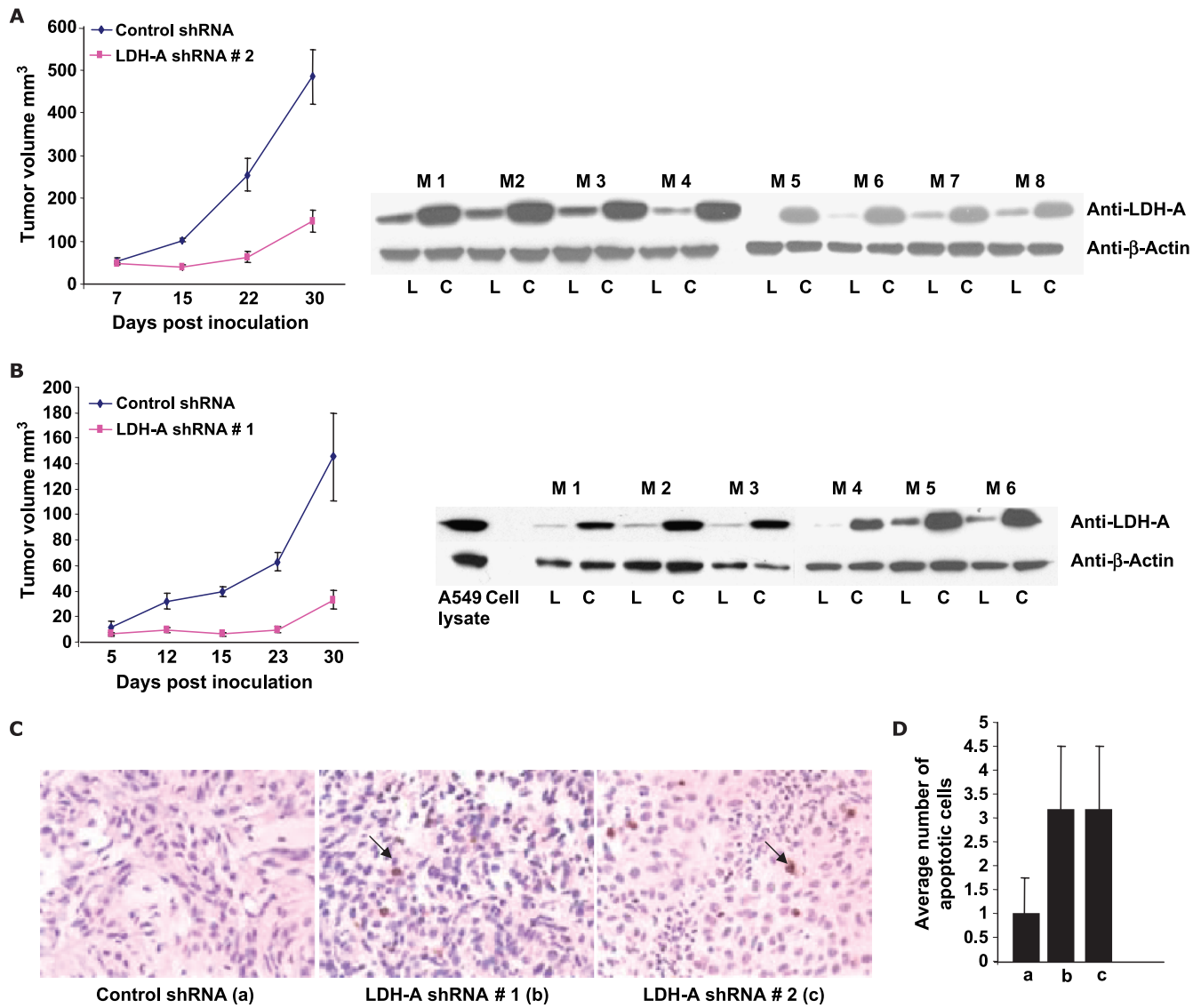


Figure 4. (A and B) Tumor growth measurements for control and A549 LDH-A-deficient cell lines in athymic mice with corresponding Western blot analysis of tumor tissue. C indicates control shRNA tumor tissue; L, LDH-A-deficient tumor tissue; M, mouse number. (C) TUNEL assay to assess apoptosis, with arrows indicating apoptotic cells. (D) Average number of apoptotic cells in four random field (20 \times) in control and LDH-A-deficient tumors by TUNEL staining. Note that in panels C and D, a refers to data with control shRNA, b refers to LDH-A shRNA no. 1, and c to LDH-A shRNA no. 2.

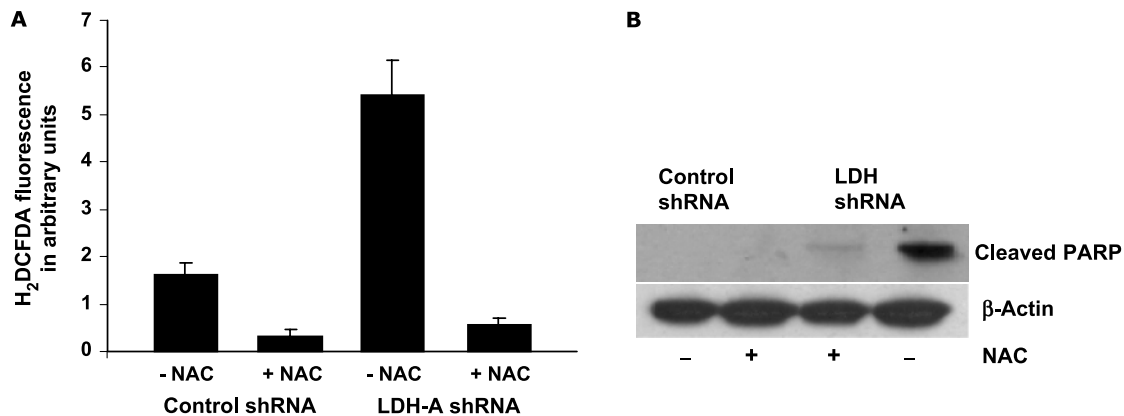


Figure 5. (A) ROS measurements by H₂DCFDA in control and LDH-A-deficient cell lines in the presence and absence of NAC. (B) Western blot analysis of cleaved PARP in control and LDH-A-deficient cells in the presence and absence of 5 mM NAC for 55 hours.

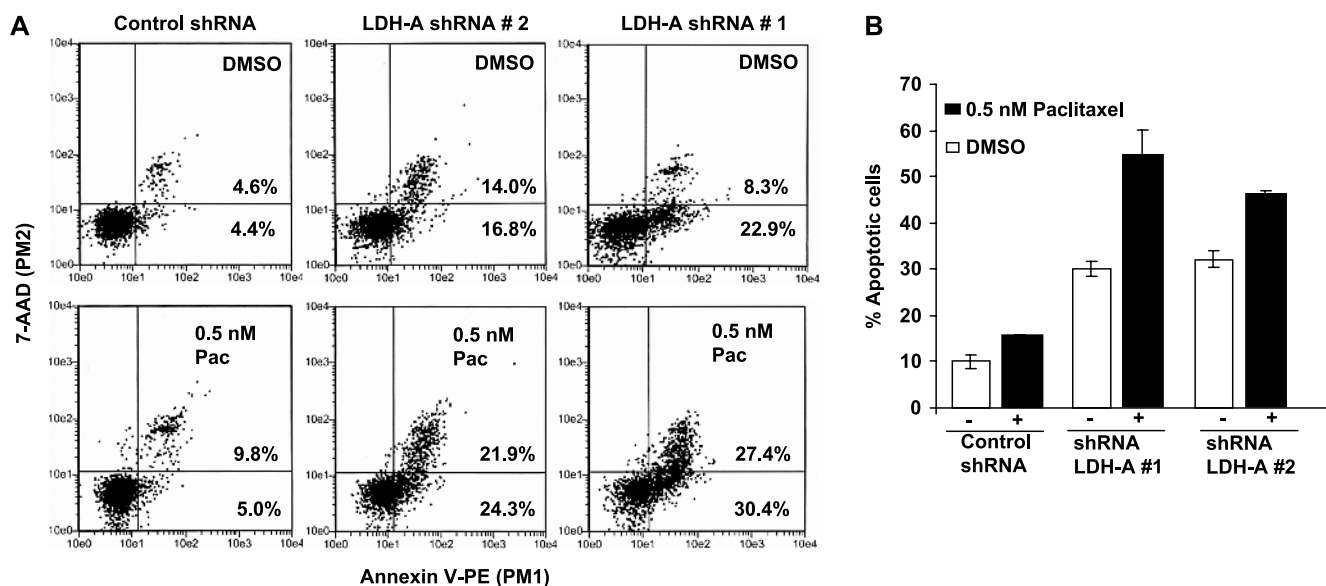


Figure 6. (A) Apoptosis measurement in control and LDH-A-deficient cells by annexin V-PE analysis in the presence or absence of 0.5 nM paclitaxel. (B) graphical representation of A.

A549 cells expressing control shRNA, in congruence with our shRNA-LDH-A findings (Figure 7).

Hyperpolarized Pyruvate Can Be Used to Monitor Changes in Metabolism In Vivo

Figure 8A displays a typical T_2 -weighted axial proton image in a tumor-bearing mouse. The bright line on the upper right indicates the center of the ^{13}C surface coil, which is situated over the tumor, indicated by the green outline. Figure 8B displays the pyruvate and lactate signals as a function of time in a pair of control (left) and DCA treated (right) mice. A reduction in lactate signal is evident in the DCA-treated tumor. Figure 8C displays a comparison of the lactate signals in eight stud-

ies performed using control tumors and in nine studies performed using tumors after DCA treatment. The values of peak lactate divided by peak pyruvate are 0.20 ± 0.07 for the control studies and 0.13 ± 0.07 for the studies with DCA treatment. A two-tailed t test yields a P value of 0.048 for the reduction in tumor lactate signal after DCA treatment.

Discussion

The findings in this report are as follows: 1) Inhibition of LDH-A in a glycolytic NSCLC tumor cell line results in ROS-mediated apoptosis and increased sensitivity to the chemotherapeutic drug paclitaxel. 2) The inhibition of fermentative glycolysis either through inhibition of

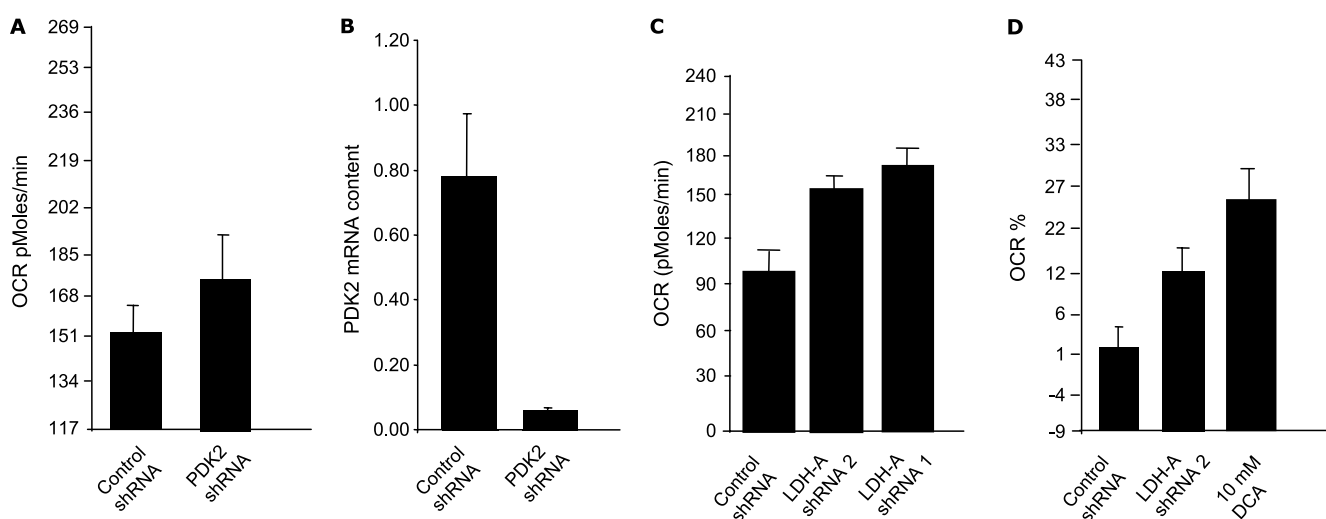


Figure 7. (A) OCR of control and A549 PDK2-deficient cell lines. (B) Real-time polymerase chain reaction analysis of control and A549 PDK2-deficient cell lines. (C) OCR of control and A549 LDH-A-deficient cell lines. (D) Comparative analysis of OCR between control and A549 LDH-A-deficient cell lines and 10 mM DCA-treated A549 cells.

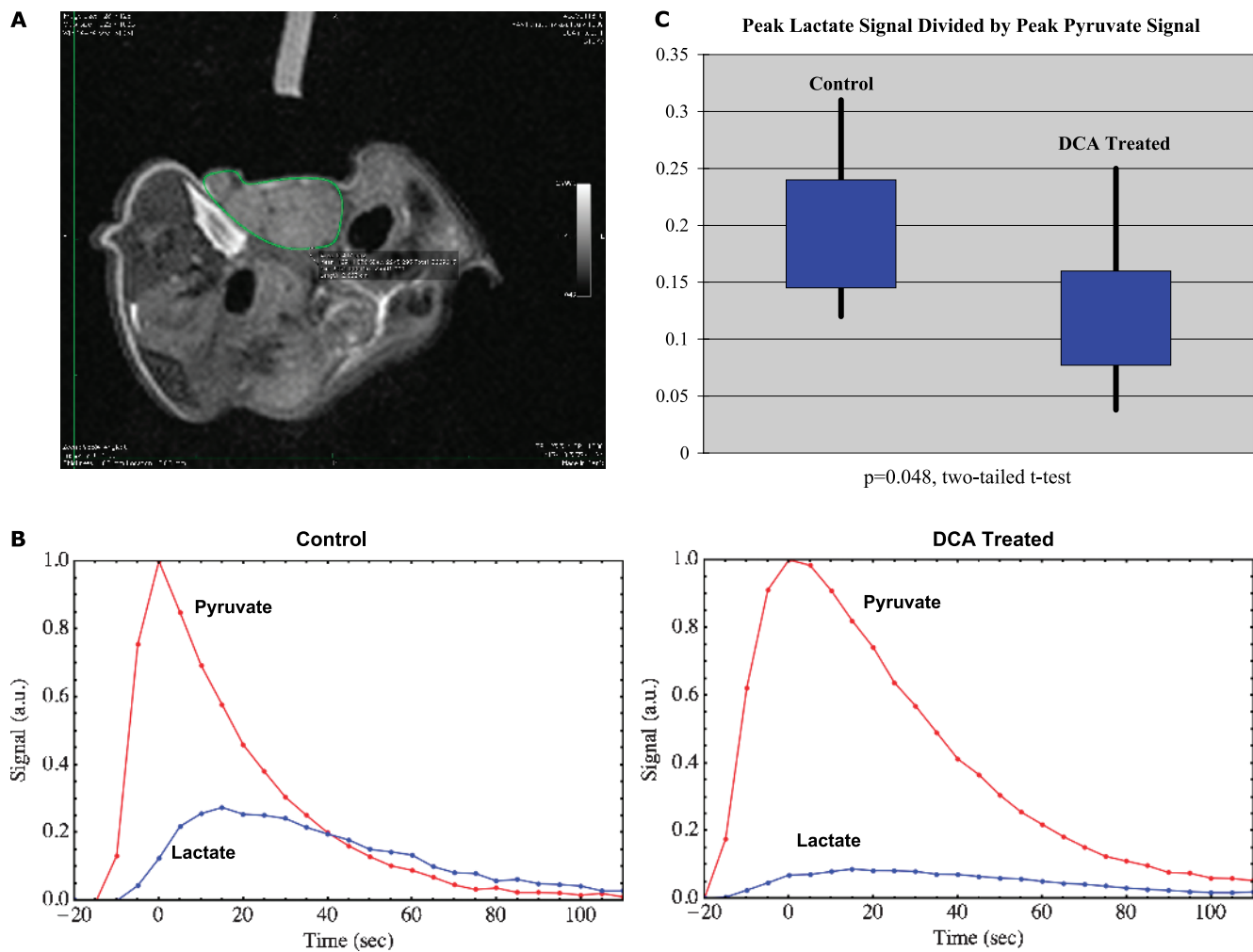


Figure 8. (A) Axial T_2 -weighted MR image of a typical tumor, outlined in green. The center axis of the ^{13}C surface coil is indicated by the bright marker at the upper left; the coil itself is situated in direct contact with the tumor. (B) Pyruvate and lactate signals acquired after administration of hyperpolarized pyruvate in representative control (left) and DCA-treated (right) tumors as a function of time. The reduction in lactate signal after DCA treatment is evident. (C) Distribution of peak lactate signal divided by peak pyruvate signal in control (left) and DCA-treated (right) tumors. The black vertical lines show the maximum and minimum values, and the blue boxes indicate the range of the second and third quartiles (i.e., the range from the 25th percentile to the 75th percentile).

LDH-A or by activation of PDH by the drug DCA can be monitored in a noninvasive real-time manner through hyperpolarized pyruvate.

Although the molecular mechanisms leading to the increased rate of glycolysis are not fully understood, it is hypothesized that enhanced conversion of pyruvate to lactate in NSCLC cells is the result of increased expression of LDH-A, a target of the *myc* oncogene [50,51] that is over-expressed in NSCLC. The expression of LDH-A is abundant in tumor cells compared with normal primary lung epithelial cells [7,8]. Moreover, LDH-A expression is also regulated by HIF-1 α [52–54] that further increases expression of LDH-A and decreases expression of PDH, which regulates pyruvate entry into TCA cycle by converting pyruvate to acetyl Co-A. The opposing effects of these two enzymes that are regulated by HIF-1 [5,55] control the glycolytic state in solid tumor environment. In the present study, we wanted to ask whether inhibition of LDH-A in the highly glycolytic NSCLC cell line A549, results in reduced tumor growth and whether it can increase the efficacy of a chemotherapeutic drug. We also asked whether we could visualize this inhibition of decreased pyruvate to lactate flux. Moreover, because of

the lack of specific LDH-A inhibitors, we asked whether the inhibition of fermentative glycolysis as measured by decreased pyruvate to lactate flux can be achieved by activation of PDH by DCA that will shuttle pyruvate toward TCA and away from LDH-A-catalyzed reaction.

To achieve these goals, we started by using RNA interference to generate stable cell lines with diminished LDH-A expression. In comparison to control cell lines, the LDH-A-deficient cell lines were still capable of proliferation under normoxic condition but at a slower rate. There was no significant difference in ATP generation in LDH-A-deficient cells compared with control cells, suggesting either that OXPHOS is functional to generate required ATP in the normoxic condition or that another LDH isoform is enough to compensate for LDH-A deficiency. However, this pattern of growth was severely restricted under hypoxic conditions with appreciable ATP depletion in LDH-A-deficient cells compared with control. It was rather surprising that the rate of proliferation for the control cell line was also retarded. We had expected that control cells would use fermentative glycolysis and show similar growth rate as observed in normoxic condition. It is possible that pH changes in

cell culture medium as a result of excess lactate production during continued hypoxia may lead to reduced cell viability. This is a key observation: LDH-A inhibition will work better under hypoxic conditions because the cells are locked into fermentative glycolysis. Therefore, we are tempted to hypothesize that cancer stem cells that tend to segregate in the hypoxic niche [56,57] and are often not affected by chemotherapy regimen, designed to inhibit rapidly proliferating cells, may be sensitive to LDH-A inhibitor therapy.

Because ATP depletion was not a likely cause of the apoptosis in the normoxic condition, and we observed increased oxygen consumption in LDH-A-deficient cells, we asked whether increased oxygen consumption leads to increased oxidative stress. We demonstrated that inhibition of LDH-A results in increased ROS generation. Moreover, the neutralization of ROS by NAC resulted in a significant reduction in cleaved PARP, suggesting that ROS may play an active role in the induction of apoptosis. The increased ROS generation by LDH-A inhibition may result from increase in electron flux in the electron transport chain and concomitant inability to efficiently transport electrons from one complex to another. These results are very similar to those demonstrating enhanced ROS production by reactivation of the TCA cycle as a result of PDH activation by DCA [20].

It has been suggested that tumors from NSCLC patients with enhanced LDH-A expression are resistant to chemotherapy treatment because of the highly acidic tumor microenvironment [8]. We wanted to ask whether inhibition of LDH-A with low lactate production will aid in enhancing the potential effect of the chemotherapy regimen. We show that LDH-A inhibition results in decreased extracellular acidification by traditional measurement of lactate content as well as by PPR measurement using the XZ-24 analyzer and that low-dose paclitaxel has an additive effect in enhancing apoptosis in LDH-A-deficient cells. These results are in line with previous studies [58] that describe markedly enhanced toxicity of paclitaxel and 2-deoxy-D-glucose in combination in NSCLC xenografts because LDH-A inhibition by directing the trafficking of pyruvate to acetyl CoA is likely to also decrease glycolytic flux as does 2-deoxy-D-glucose.

Many cancer drugs often exhibit toxicity in nonmalignant tissues, partly because their targets are also expressed in these tissues. Inhibition of LDH-A makes it an attractive target in cancer therapy because its expression is largely relegated to the skeletal muscle. Moreover, humans with LDH-A deficiency show a relatively normal phenotype and exhibit myoglobinuria under intense anaerobic exercising. Moreover, LDH-A inhibition may be better suited in combination with chemotherapeutic regimen because most of the current therapies are inadequate to target hypoxic region that may potentially harbor stem cells. Thus, the development of inhibitors of LDH-A makes eminent sense for the treatment of a potentially large group of cancers in which the Warburg effect is operational, perhaps as many as 60% to 80% of tumor types.

Our demonstration that inhibition of fermentative glycolysis by small molecule inhibitor can be imaged noninvasively and in real time may allow for a novel surrogate clinical end point: the capacity to monitor the fate of pyruvate. Thus, dosing and scheduling of DCA administration can be optimized for maximal effects on changes in pyruvate flux rather than being governed by toxicity end points. Such a capacity could provide valuable first-in-human data for drugs that target the fate of pyruvate and aim to reverse the Warburg effect: drugs that either inhibit LDH-A or enhance the PDH complex. This capability can streamline development of this drug class and potentially reduce costs by providing early “go, no go” decisions that are mechanistically based. The proposed technology—use of hyperpolarized MRI—is scalable to human use and

has broad applicability in this regard because most solid tumors exhibit the Warburg effect.

References

- Gatenby RA and Gillies RJ (2004). Why do cancers have high aerobic glycolysis? *Nat Rev Cancer* **4**, 891–899.
- Iliopoulos O, Kibel A, Gray S, and Kaelin WG Jr (1995). Tumour suppression by the human von Hippel-Lindau gene product. *Nat Med* **1**, 822–826.
- Isaacs JS, Jung YJ, Mole DR, Lee S, Torres-Cabala C, Chung YL, Merino M, Trepel J, Zbar B, Toro J, et al. (2005). HIF overexpression correlates with biallelic loss of fumarate hydratase in renal cancer: novel role of fumarate in regulation of HIF stability. *Cancer Cell* **8**, 143–153.
- Pouyssegur J, Dayan F, and Mazure NM (2006). Hypoxia signalling in cancer and approaches to enforce tumour regression. *Nature* **441**, 437–443.
- Kim JW, Tchernyshyov I, Semenza GL, and Dang CV (2006). HIF-1-mediated expression of pyruvate dehydrogenase kinase: a metabolic switch required for cellular adaptation to hypoxia. *Cell Metab* **3**, 177–185.
- Matoba S, Kang JG, Patino WD, Wragg A, Boehm M, Gavrilova O, Hurley PJ, Bunz F, and Hwang PM (2006). p53 regulates mitochondrial respiration. *Science* **312**, 1650–1653.
- Koukourakis MI, Giatromanolaki A, Polychronidis A, Simopoulos C, Gatter KC, Harris AL, and Sivridis E (2006). Endogenous markers of hypoxia/anaerobic metabolism and anemia in primary colorectal cancer. *Cancer Sci* **97**, 582–588.
- Koukourakis MI, Giatromanolaki A, and Sivridis E (2003). Lactate dehydrogenase isoenzymes 1 and 5: differential expression by neoplastic and stromal cells in non-small cell lung cancer and other epithelial malignant tumors. *Tumour Biol* **24**, 199–202.
- Koukourakis MI, Giatromanolaki A, Sivridis E, Bougioukas G, Didilis V, Gatter KC, and Harris AL (2003). Lactate dehydrogenase-5 (LDH-5) overexpression in non-small-cell lung cancer tissues is linked to tumour hypoxia, angiogenic factor production and poor prognosis. *Br J Cancer* **89**, 877–885.
- Jungmann RA, Huang D, and Tian D (1998). Regulation of LDH-A gene expression by transcriptional and posttranscriptional signal transduction mechanisms. *J Exp Zool* **282**, 188–195.
- Jungmann RA and Kiryukhina O (2005). Cyclic AMP and AKAP-mediated targeting of protein kinase A regulates lactate dehydrogenase subunit A mRNA stability. *J Biol Chem* **280**, 25170–25177.
- Dimmer KS, Friedrich B, Lang F, Deitmer JW, and Broer S (2000). The low-affinity monocarboxylate transporter MCT4 is adapted to the export of lactate in highly glycolytic cells. *Biochem J* **350**(pt 1), 219–227.
- Ullah MS, Davies AJ, and Halestrap AP (2006). The plasma membrane lactate transporter MCT4, but not MCT1, is up-regulated by hypoxia through a HIF-1 α -dependent mechanism. *J Biol Chem* **281**, 9030–9037.
- Fantin VR, St-Pierre J, and Leder P (2006). Attenuation of LDH-A expression uncovers a link between glycolysis, mitochondrial physiology, and tumor maintenance. *Cancer Cell* **9**, 425–434.
- Xie H, Valera VA, Merino MJ, Amato AM, Signoretti S, Linehan WM, Sukhatme VP, and Seth P (2009). LDH-A inhibition, a therapeutic strategy for treatment of hereditary leiomyomatosis and renal cell cancer. *Mol Cancer Ther* **8**, 626–635.
- Stacpoole PW (1989). The pharmacology of dichloroacetate. *Metabolism* **38**, 1124–1144.
- Michelakis ED, Webster L, and Mackey JR (2008). Dichloroacetate (DCA) as a potential metabolic-targeting therapy for cancer. *Br J Cancer* **99**, 989–994.
- Stacpoole PW (1969). Review of the pharmacologic and therapeutic effects of diisopropylammonium dichloroacetate (DIPA). *J Clin Pharmacol J New Drugs* **9**, 282–291.
- Stacpoole PW, Nagaraja NV, and Hutson AD (2003). Efficacy of dichloroacetate as a lactate-lowering drug. *J Clin Pharmacol* **43**, 683–691.
- Bonnet S, Archer SL, Allalunis-Turner J, Haromy A, Beaulieu C, Thompson R, Lee CT, Lopaschuk GD, Puttagunta L, Bonnet S, et al. (2007). A mitochondria-K⁺ channel axis is suppressed in cancer and its normalization promotes apoptosis and inhibits cancer growth. *Cancer Cell* **11**, 37–51.
- Cao W, Yacoub S, Shiverick KT, Namiki K, Sakai Y, Porvasnik S, Urbanek C, and Rosser CJ (2008). Dichloroacetate (DCA) sensitizes both wild-type and overexpressing Bcl-2 prostate cancer cells *in vitro* to radiation. *Prostate* **68**, 1223–1231.
- Golman K, Axelsson O, Johannesson H, Mansson S, Olofsson C, and Pettersson JS (2001). Parahydrogen-induced polarization in imaging: subsecond ¹³C angiography. *Magn Reson Med* **46**, 1–5.

- [23] Golman K, Ardenkjaer-Larsen JH, Svensson J, Axelsson O, Hansson G, Hansson L, Johannesson H, Leunbach I, Mansson S, Petersson JS, et al. (2002). ^{13}C -angiography. *Acad Radiol* **9**(suppl 2), S507–S510.
- [24] Kohler S, Yen Y, Wolber J, Chen AP, Albers MJ, Bok R, Zhang V, Tropp J, Nelson S, Vigneron D, et al. (2007). *In vivo* C13 metabolic imaging at 3T with hyperpolarized C13-1-pyruvate. *Magn Reson Med* **58**, 65–69.
- [25] Day SE, Kettunen MI, Gallagher FA, Hu D-E, Lerche MH, Wolber J, Golman K, Ardenkjaer-Larsen JH, and Brindle KM (2007). Detecting tumor response to treatment using hyperpolarized ^{13}C magnetic resonance imaging and spectroscopy. *Nat Med* **13**, 1382–1387.
- [26] Kettunen MI, Hu DE, Whitney TH, McLaughlin R, Gallagher FA, Bohndiek SE, Day SE, and Brindle KM (2010). Magnetization transfer measurements of exchange between hyperpolarized $[1-^{13}\text{C}]$ pyruvate and $[1-^{13}\text{C}]$ lactate in a murine lymphoma. *Magn Reson Med* **63**, 872–880.
- [27] Harris T, Eliyahu G, Frydman L, and Degani H (2009). Kinetics of hyperpolarized C13-pyruvate transport and metabolism in living human breast cancer cells. *Proc Natl Acad Sci USA* **106**, 18131–18136.
- [28] Albers MJ, Bok R, Chen AP, Cunningham CH, Zierhut ML, Zhang V, Kohler S, Tropp J, Hurd RE, Yen Y, et al. (2008). Hyperpolarized ^{13}C lactate, pyruvate, and alanine: noninvasive biomarkers for prostate cancer detection and grading. *Cancer Res* **68**, 8607–8615.
- [29] Ward CS, Venkatesh HS, Chaumeil MM, Brandes AH, Vancricking M, Dafni H, Sukumar S, Nelson SJ, Vigneron DB, Kurhanewicz J, et al. (2010). Noninvasive detection of target modulation following phosphatidylinositol 3-kinase inhibition using hyperpolarized ^{13}C magnetic resonance spectroscopy. *Cancer Res* **70**, 1296–1305.
- [30] Gallagher FA, Kettunen MI, Hu DE, Jensen PR, Zandt R, Karlsson M, Gisselsson A, Nelson SK, Whitney TH, Bohndiek SE, et al. (2009). Production of hyperpolarized $[1,4-^{13}\text{C}_2]$ malate from $[1,4-^{13}\text{C}_2]$ fumarate is a marker of cell necrosis and treatment response in tumors. *Proc Natl Acad Sci USA* **106**, 19801–19806.
- [31] Kurdzesau F, van den Brandt B, Comment A, Hautle P, Jannin S, van der Klink JJ, and Kontar JA (2008). Dynamic nuclear polarization of labeled molecules in frozen water-alcohol solutions. *J Phys D Appl Phys* **41**, 155506–155516.
- [32] Bhattacharya P, Chekmenov EY, Perman W, Harris KC, Lin AP, Norton VA, Tan CC, Ross BD, and Weitekamp DP (2007). Toward hyperpolarized imaging of C13-succinate imaging of brain cancer. *J Magn Reson* **186**, 150–155.
- [33] Gabellieri C, Reynolds S, Lavie A, Payne GS, Leach MO, and Eykyn TR (2008). Therapeutic target metabolism observed using hyperpolarized 15N choline. *J Am Chem Soc* **128**, 4526–4527.
- [34] Keshari KR, Wilson DM, Chen AP, Bok R, Larson PEZ, Hu S, Van Crielinge M, Macdonald JM, Vigneron DB, and Kurhanewicz J (2009). Hyperpolarized $[2-^{13}\text{C}]$ fructose: a hemiketal DNP substrate for *in vivo* metabolic imaging. *J Am Chem Soc* **131**, 17591–17596.
- [35] Root DE, Hacohen N, Hahn WC, Lander ES, and Sabatini DM (2006). Genome-scale loss-of-function screening with a lentiviral RNAi library. *Nat Methods* **3**, 715–719.
- [36] Rhee I, Bachman KE, Park BH, Jair KW, Yen RW, Schuebel KE, Cui H, Feinberg AP, Lengauer C, Kinzler KW, et al. (2002). DNMT1 and DNMT3b cooperate to silence genes in human cancer cells. *Nature* **416**, 552–556.
- [37] Thangaraju M, Carswell KN, Prasad PD, and Ganapathy V (2009). Colon cancer cells maintain low levels of pyruvate to avoid cell death caused by inhibition of HDAC1/HDAC3. *Biochem J* **417**, 379–389.
- [38] Leiblich A, Cross SS, Catto JW, Phillips JT, Leung HY, Hamdy FC, and Rehman I (2006). Lactate dehydrogenase-B is silenced by promoter hypermethylation in human prostate cancer. *Oncogene* **25**, 2953–2960.
- [39] Lu H, Forbes RA, and Verma A (2002). Hypoxia-inducible factor 1 activation by aerobic glycolysis implicates the Warburg effect in carcinogenesis. *J Biol Chem* **277**, 23111–23115.
- [40] Wu M, Neilson A, Swift AL, Moran R, Tamagnine J, Parslow D, Armistead S, Lemire K, Orrell J, Teich J, et al. (2007). Multiparameter metabolic analysis reveals a close link between attenuated mitochondrial bioenergetic function and enhanced glycolysis dependency in human tumor cells. *Am J Physiol Cell Physiol* **292**, C125–C136.
- [41] Ananth S, Knebelmann B, Gruning W, Dhanabal M, Walz G, Stillman IE, and Sukhatme VP (1999). Transforming growth factor β 1 is a target for the von Hippel-Lindau tumor suppressor and a critical growth factor for clear cell renal carcinoma. *Cancer Res* **59**, 2210–2216.
- [42] Poon E, Clermont F, Firpo MT, and Akhurst RJ (2006). TGF β inhibition of yolk-sac-like differentiation of human embryonic stem-cell-derived embryoid bodies illustrates differences between early mouse and human development. *J Cell Sci* **119**, 759–768.
- [43] Brizel DM, Schroeder T, Scher RL, Walenta S, Clough RW, Dewhurst MW, and Mueller-Klieser W (2001). Elevated tumor lactate concentrations predict for an increased risk of metastases in head-and-neck cancer. *Int J Radiat Oncol Biol Phys* **51**, 349–353.
- [44] Burk D, Woods M, and Hunter J (1967). On the significance of glycolysis for cancer growth, with special reference to Morris rat hepatomas. *J Natl Cancer Inst* **38**, 839–863.
- [45] Fischer K, Hoffmann P, Voelkl S, Meidenbauer N, Ammer J, Edinger M, Gottfried E, Schwarz S, Rothe G, Hoves S, et al. (2007). Inhibitory effect of tumor cell-derived lactic acid on human T cells. *Blood* **109**, 3812–3819.
- [46] Gottfried E, Kunz-Schughart LA, Ebner S, Mueller-Klieser W, Hoves S, Andreesen R, Mackensen A, and Kreutz M (2006). Tumor-derived lactic acid modulates dendritic cell activation and antigen expression. *Blood* **107**, 2013–2021.
- [47] Lardner A (2001). The effects of extracellular pH on immune function. *J Leukoc Biol* **69**, 522–530.
- [48] Trowell OA (1953). The effect of environmental factors on the radiosensitivity of lymph nodes cultured *in vitro*. *Br J Radiol* **26**, 302–309.
- [49] Mahoney BP, Raghunand N, Baggett B, and Gillies RJ (2003). Tumor acidity, ion trapping and chemotherapeutics: I. Acid pH affects the distribution of chemotherapeutic agents *in vitro*. *Biochem Pharmacol* **66**, 1207–1218.
- [50] Osthus RC, Shim H, Kim S, Li Q, Reddy R, Mukherjee M, Xu Y, Woney D, Lee LA, and Dang CV (2000). Deregulation of glucose transporter 1 and glycolytic gene expression by c-Myc. *J Biol Chem* **275**, 21797–21800.
- [51] Shim H, Dolde C, Lewis BC, Wu CS, Dang G, Jungmann RA, Dalla-Favera R, and Dang CV (1997). c-Myc transactivation of LDH-A: implications for tumor metabolism and growth. *Proc Natl Acad Sci USA* **94**, 6658–6663.
- [52] Firth JD, Ebert BL, and Ratcliffe PJ (1995). Hypoxic regulation of lactate dehydrogenase A. Interaction between hypoxia-inducible factor 1 and cAMP response elements. *J Biol Chem* **270**, 21021–21027.
- [53] Semenza GL, Roth PH, Fang HM, and Wang GL (1994). Transcriptional regulation of genes encoding glycolytic enzymes by hypoxia-inducible factor 1. *J Biol Chem* **269**, 23757–23763.
- [54] Semenza GL, Rue EA, Iyer NV, Pang MG, and Kearns WG (1996). Assignment of the hypoxia-inducible factor 1 α gene to a region of conserved synteny on mouse chromosome 12 and human chromosome 14q. *Genomics* **34**, 437–439.
- [55] Papandreou I, Cairns RA, Fontana L, Lim AL, and Denko NC (2006). HIF-1 mediates adaptation to hypoxia by actively downregulating mitochondrial oxygen consumption. *Cell Metab* **3**, 187–197.
- [56] Das B, Tsuchida R, Malkin D, Koren G, Baruchel S, and Yeger H (2008). Hypoxia enhances tumor stemness by increasing the invasive and tumorigenic side population fraction. *Stem Cells* **26**, 1818–1830.
- [57] Keith B and Simon MC (2007). Hypoxia-inducible factors, stem cells, and cancer. *Cell* **129**, 465–472.
- [58] Maschek G, Savaraj N, Priebe W, Braunschweiger P, Hamilton K, Tidmarsh GF, De Young LR, and Lampidis TJ (2004). 2-Deoxy-D-glucose increases the efficacy of adriamycin and paclitaxel in human osteosarcoma and non-small cell lung cancers *in vivo*. *Cancer Res* **64**, 31–34.